Chapter

Experimental Aspects of Holographic Projection with a Liquid-Crystal-on-Silicon Spatial Light Modulator

Michal Makowski

Abstract

Dynamic electroholography is a suitable and promising technology of image display for future projection and near-eye displays. Until a new phase modulation technology is introduced, practical research assumes the use of pixelated spatial light modulators based on liquid crystals with electronically controlled birefringence leading to a controllable refractive index. Such an approach allows for university grade development and testing of holographic computation methodology, but its limitations and drawbacks currently disable the massive application in consumer electronics. This chapter describes the differences between the behavior of the modulator as expected from Fourier optics and that observed in practical optical experiments. Moreover, practical hints and proven techniques of overcoming selected hardware issues of the chosen liquid-crystal-on-silicon (LCoS) phase modulators are given. The smart combination of the described techniques could allow more precise operation of spatial light modulators with a higher agreement with numerical simulations, especially for holographic projection of colorful images.

Keywords: holography, Fourier optics, spatial light modulator, projection, computer-generated holography

1. Introduction

Modern flat-screen liquid crystal and organic light emitting diode (OLED) displays grow in size and resolution; nevertheless, the optimal technology for even larger screens is still based on projection. The basic principle is that the real image is formed on the surface of a screen, which reflects and diffuses the intensity field toward the viewers, as it happens in cinemas and home theater systems. Image projection based on the classical optical approach utilizing lenses, high-powered lamps, and intensity modulation (e.g., DMD—digital micromirror device, DLP—digital light processing, LC—liquid crystal, or a celluloid tape) has not changed much since its invention and still has numerous disadvantages. It suffers from extremely low efficiency, which means that most of the light is converted into heat, which involves noisy, active cooling. It requires high-quality lenses to avoid visible optical aberrations—both geometrical and chromatic. Most of all, the size

of the optical setup cannot be freely down-sized due to the physical requirements of the imaging process and the number and size of the apertures of the lenses. For example, shrinking the main imaging lens causes unavoidable loss of resolution due to light diffraction on the aperture of the lens. For those reasons, the image projection drifts toward the holographic image forming technique [1, 2], which is covered in this chapter.

From the practical point of view, one expects superior efficiency combined with excellent image quality and refresh rate. All those demands can be met from the theoretical point of view. The lens-less image forming by phase modulation of light with a spatial light modulator (SLM) theoretically gives 100% efficiency and allows any size of the final image, without any aberrations, noise and with real-time refresh on very large screens. Obviously, the main aspect that differ the theory from the experimental results is the hardware constraints and limitations of the SLMs currently available on the market [3]. To name a few of those aspects: the limited time response of the liquid crystal, the pixelated structure of the SLM, the non-100% fill factor, limited pixel count, lack of optical flatness, etc. [4]. Until now, better techniques of phase modulation are introduced, and one can overcome and suppress the consequences of those drawbacks of current SLMs by applying selected concepts presented in this chapter. The following subchapters will describe the experimentally validated methods of tweaking of the SLM response for the needs of good experimental realization of electro-holographic projection of 2-D images. This chapter covers only the techniques tested and experimentally proven by the author's research group. Obviously, the reader may find numerous other methods in the literature, often superior to the ones listed here.

2. The representation of a liquid crystal on silicon spatial light modulator in Fourier optics

2.1 Cartesian pixelated structure of the SLM

From the point of view of Fourier optics, the spatial light modulator provides the ability of creating a phase-only spatial 2-D field, composed of (usually square-shaped) pixels, which are associated with samples. From the mathematical point of view, the samples should contain the value of the field in their location, and moreover, they should be infinitesimally small. The pixels of popular SLMs are in the range of 8–3.74 μm and have the shape of a square. The phase retardation is the same in the whole area of the pixel, which is a major difference from the case of point-sized samples in the Fourier approach.

The nonzero size of SLM pixels greatly influences the nature of the formed optical fields, which is especially visible in their Fourier transforms. In order to illustrate that, let us assume the simplest optical realization of the Fourier transform with a converging wave illuminating the SLM, as shown in **Figure 1**.

The field reflected from the SLM carries the phase of a computer-generated hologram (CGH), therefore when the convergent beam reaches its waist, the Fourier transform of the hologram is reconstructed as an intensity field. Since the hologram was Fourier-type, the exemplary encoded image of a *Rubik cube* appears in the Fourier plane.

As seen in **Figure 2**, the hologram (signal g) displayed on the SLM must be treated as a set of samples (ergo the *combus* function) convolved with the *rect* function, which defines the shape of an individual pixel of the SLM. Therefore, the Fourier transform of such field, observed at the screen, is composed of:

- The central image (G), being an intensity Fourier transform of the input signal g.

- Copies of the G signal being the result of the convolution with the comb function.

The angular periodicity of the duplicates is governed by the law of diffraction:

$$\alpha_{diff} = \arcsin\left(\frac{m\lambda}{p}\right) \tag{1}$$

where m is the growing order numbering subsequent duplicates in a chosen direction x or y, and p is the pixel pitch of the SLM.

2.2 Pixel shape and intensity envelope

For technical reasons, the active (phase modulating) area of each pixel does not occupy 100% of the pixel's surface. The presence of residual static (non-modulating) interpixel gap accounts for the non-100% fill factor (FF) of a given SLM, defined as the ratio of the active surface of the SLM to the whole surface of

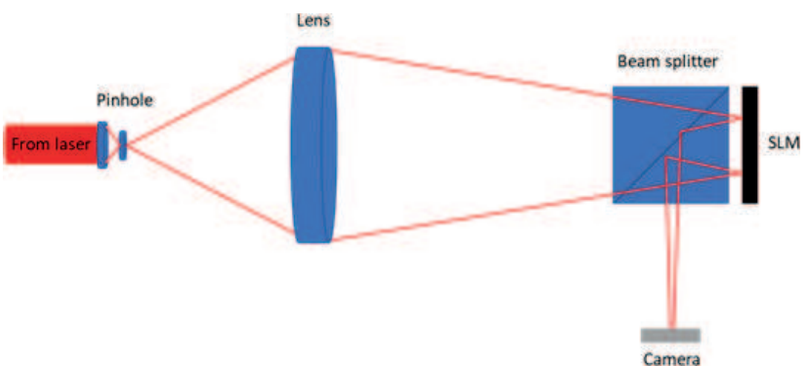

Figure 1.
Scheme of a typical optical setup for holographic projection. Only border light rays without refraction are shown for clarity.

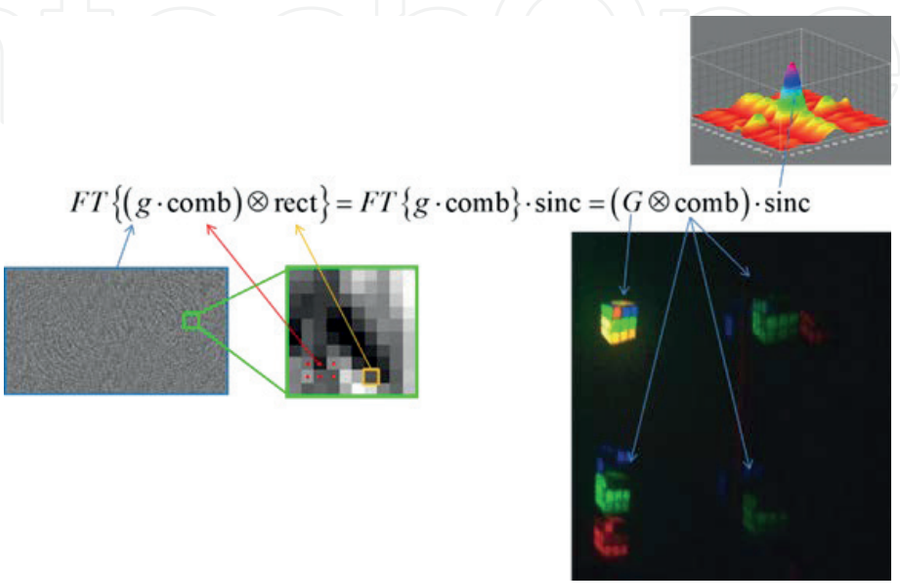

Figure 2.
Components of the Fourier transform of an input field g displayed on a pixelated SLM.

the SLM. Typically, this value is within the range of 80–95% (e.g., 87% for Holoeye Pluto-1, 93% for Holoeye Pluto-2, 90% for Holoeye GAEA) and tends to rise for lower pixel pitch values, due to minimal width of the interpixel lines in CMOS technology.

The intensity pattern visible in **Figure 2** is attenuated by the so-called intensity envelope, denoted as *sinc*. Its shape in first approximation is the Fourier transform of the shape of an individual pixel of the SLM. For square-shaped pixels, the amplitude of the envelope function is: $\mathrm{sinc}(x) = \sin(x)/x$. The attenuation of the central usable image is rather straightforward to take into account at the stage of computation of the CGH. Simply, the input image must be edited in a way that its central regions are artificially darkened so as to overexpose the boundary regions in the projection [5].

The minima of the *sinc* envelope have the position determined by the size of the *rect* function describing the active (phase modulating) part of the individual pixel, for example, 7.7 μm in **Figure 3**. For FF = 100%, the pixel pitch and the pixel size are equal, which luckily results in the minima of the attenuating function falling in the central locations of the duplicate intensity patterns, as shown in **Figure 4a**.

For any value of FF lower than 100%, the mismatch of the mentioned two functions causes the increased visibility of the spurious copies, often referred to as *higher order images*, as seen in **Figure 4b**. Therefore, the limited fill factor boosts the visibility of useless higher orders and takes the energy away from the useful first diffractive order (the central one in **Figure 2**).

2.3 Spurious orders of diffraction

The replicas of colorful holographically projected fields disappear when the angle of diffraction of the blue light in the second diffractive order reaches 90°, that is, for the pixel pitch of the SLM equal to the wavelength (e.g., 445 nm). Currently, available state of the art SLMs has the pixel pitch as large as 3.74 μm, therefore such a straightforward method of mitigation of higher orders will be the matter of distant future.

The formation of the stray higher orders of diffraction is especially problematic in holographic translucent displays, where duplicates of virtual images are created in the peripheral areas of the user's view, often with a noticeable color breakup—see **Figure 2**. They are easily perceivable and difficult to obstruct

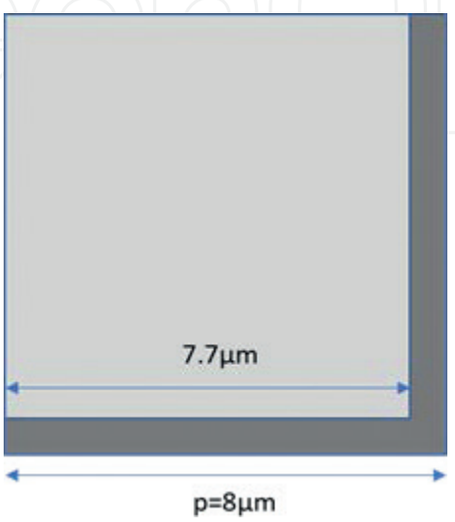

Figure 3.
Conceptual scheme of an individual pixel of a spatial light modulator for p = 8 μm and fill factor = 93%. Active pixel area is shown in light gray, interpixel gap is shown in dark gray.

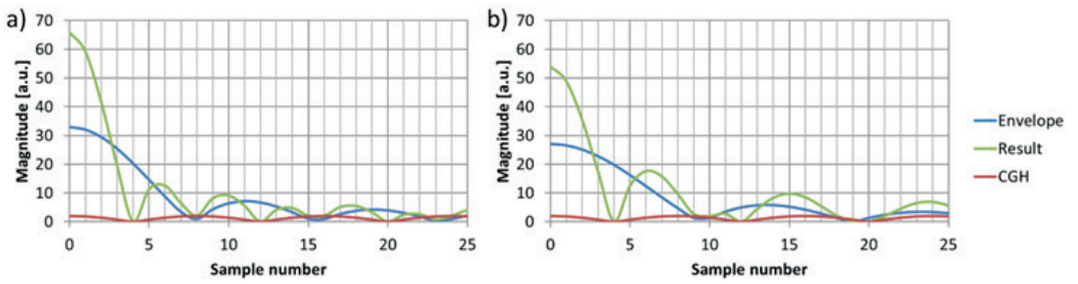

Figure 4.
Sinc envelope functions (blue) and resulting amplitude of holographic images for (a) pixel pitch equal to pixel size and (b) mismatch at 17%.

without a significant increase in the complexity or size of the optical setup. In larger experimental setups, for example, in the far-field holographic projection of 2-D intensity patterns, one can easily use filtering of the Fourier spectrum [6], as presented in **Figure 5**.

With this technique, one can efficiently filter out higher diffractive orders and additionally zero diffractive order, which is understood as the light that was not successfully modulated by the SLM. Depending on the size of the optical setup, the placement and transparency of the filter must be precisely matched to the beam; therefore, one of the proposed techniques is the photographic in-situ exposure and development of a perfectly matched filter [7], presented in **Figure 6**.

The advantage of this method is that it allows virtually all spatial frequencies achievable by the SLM to be used for image projection, except for the zero frequency. On the other hand, it requires a long optical path and access to the Fourier plane, which is usually problematic in compact devices.

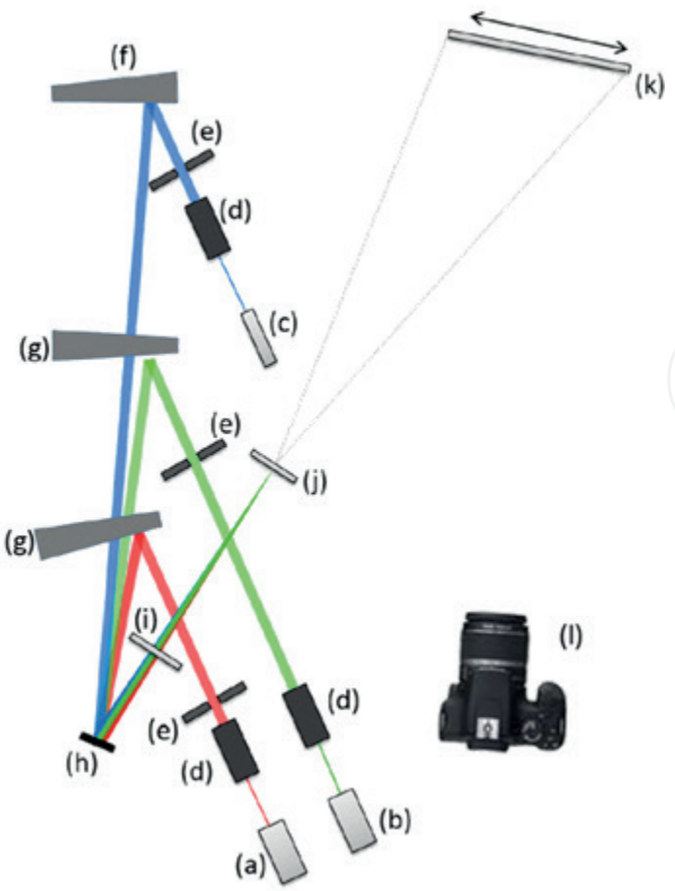

Figure 5.
Experimental setup of holographic projection with filtration in the Fourier domain [7].

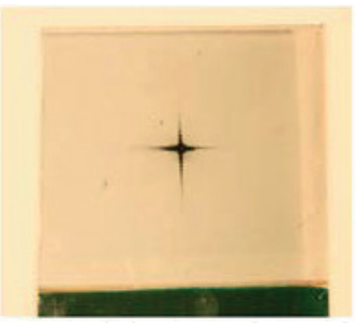

Figure 6.
Matched Fourier-plane filter, exposed and developed in the optical path [7].

3. Illumination of the SLM in compact optical setups

In long-distance projection, one has the freedom of choosing the scheme of illumination of the SLM. Typically, one can use a beam splitter configuration, as shown in **Figure 1**, for the price of the loss of c.a. 75% of the light by two passes through the cube. If the energetic efficiency and elimination of stray light is the critical factor, the more suitable illumination scheme is the tilted mode presented in **Figure 5**, where the inclined beams are colinearly reflected from the SLM at angles derived from the equation of a diffractive grating. Obviously, for larger angles of incidence, the SLM will introduce astigmatism, as a result of a slightly denser effective pixel structure in one direction. This can be taken into account by multiplication of the displayed CGHs, for eample, with the phase pattern of a properly matched cylindrical lens or by applying phase correction by calculation based on Zernike coefficients. Nevertheless, the above mentioned simple techniques are of little importance in compact projection setups designed for near-eye displays and other portable, lightweight devices. The projection in such setups typically assumes the formation of a real image inside the device, which means projection distances of roughly few centimeters. The theoretical minimal projection (focusing) distance of an SLM with a pixel pitch of p and aperture of D is given by [5]:

$$z = \frac{D}{2\tan\left(\arcsin\frac{\lambda}{2p}\right)} \tag{2}$$

In order to decrease the aforementioned distance, one can increase the optical power of the SLM by adding a physical lens in the plane of the modulator, as shown in **Figure 7**. In addition, a more compact light source can be used in a form of a polarization-maintaining (PM) single-mode optical fiber with the coupled

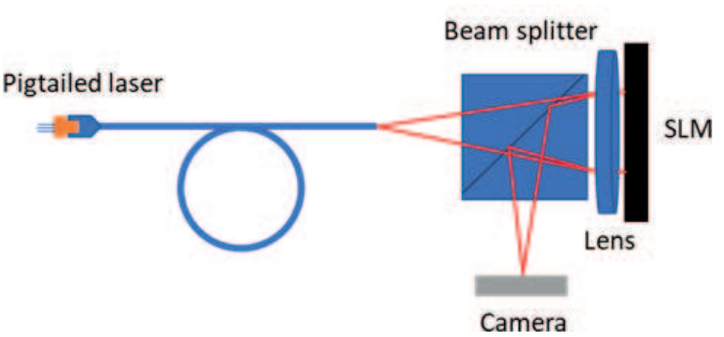

Figure 7.
Compact illumination scheme of the SLM with additional focusing lens.

laser diode. Due to the small diameter of the fiber's core, such a light source can be treated as quasi-point, yielding diffraction-limited imaging resolutions.

The advantage of this method is that as a result of almost zero distance between the SLM and the focusing lens, they can be treated as a single lens with easily adjustable focal power. As a result, the combined optical aberrations of such a tandem can be easily corrected with proper phase masks displayed on the SLM. Therefore, virtually aberration-less imaging can be realized in an extremely small configuration.

The use of a beam splitter allows the proper SLM incidence angle of zero degrees but wastes most of the energy of the light source to stray light. The below configuration shown in **Figure 8** helps to overcome this problem for the price of using custom-designed free-form optics [8].

The freeform prism is illuminated with a divergent beam from a bare laser diode equipped with a half plate for the control of polarization. The angles are matched so as the rays are reflected from the curved upper surface of the prism according to the rule of a total internal reflection (TIR). The reflected wave has lower divergence as if it has been transformed by a concave mirror. The beam that reaches the SLM has an incidence angle of almost zero degrees; therefore, the optimal conditions of phase modulation are met. The wave reflected from the SLM passes through the prism, again being focused at the exit to the air by the

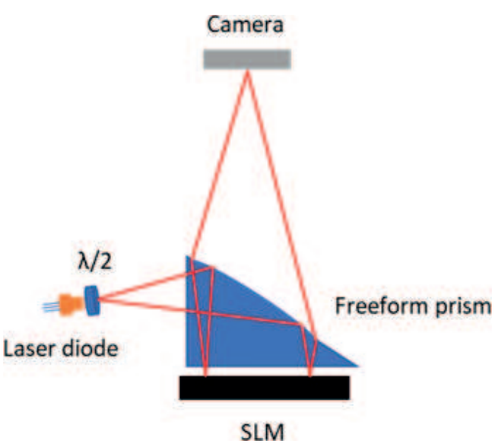

Figure 8.
Side illumination of the SLM with freeform prism and the utilization of the total internal reflection [8].

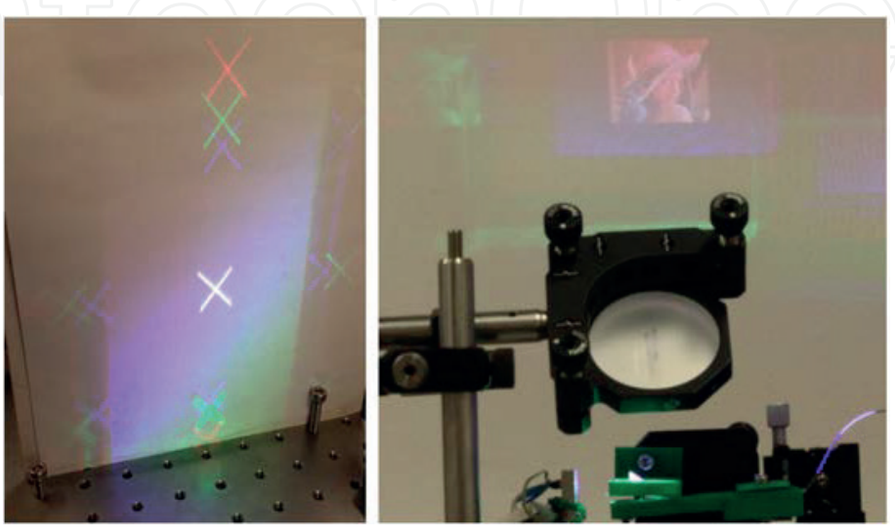

Figure 9.
Experimental realization of miniature projection head with side illumination allows efficient color projection in ambient lighting conditions [8].

curved interface of the prism. The exit beam has collimated nature, which can be easily changed to a convergent one by adding small optical power by the SLM. For this reason, the depicted setup is suitable for far-field long distance projection with extremely small and efficient optical setup, as seen in the practical realization shown in **Figure 9**.

4. Computation of computer-generated holograms

In the Fourier holographic projection configuration, shown in **Figures 1,** 7 and **8**, the projected image is the intensity Fourier transform of the field rendered by the SLM. In practical situations when asymmetrical images are played back on the screen, the SLM would have to form a complex field, which is currently impossible, unless methods of complex modulation on double SLMs are used, see subchapter "Complex modulation method".

4.1 Random and ordered phase approach

For phase-only SLMs, the amplitude part of a complex field is discarded; therefore, the main function of the CGH computation algorithms is the transfer of object information from a complex field to the phase domain. Two of the most general and universal algorithms: Gerchberg-Saxton (GS) [45] and Random Phase Free [9]—assume that initially the phase domain of the hologram is filled with spatial frequencies that should form a quasi-uniform intensity at the projection plane. In the next step, the algorithms in an iterative loop let the phase evolve freely by cyclical applications of amplitude constraints in the image plane and in the SLM plane. The main difference between the mentioned algorithms is the character of the initial phase. It is random in the G-S algorithm and ordered in the RPF algorithm, nevertheless, both configurations simulate physically feasible situations, depicted in **Figure 10** [10].

In the random phase approach (G-S), the CGH on the SLM is supposed to contain all the spatial frequencies that allow each point of the image to be created

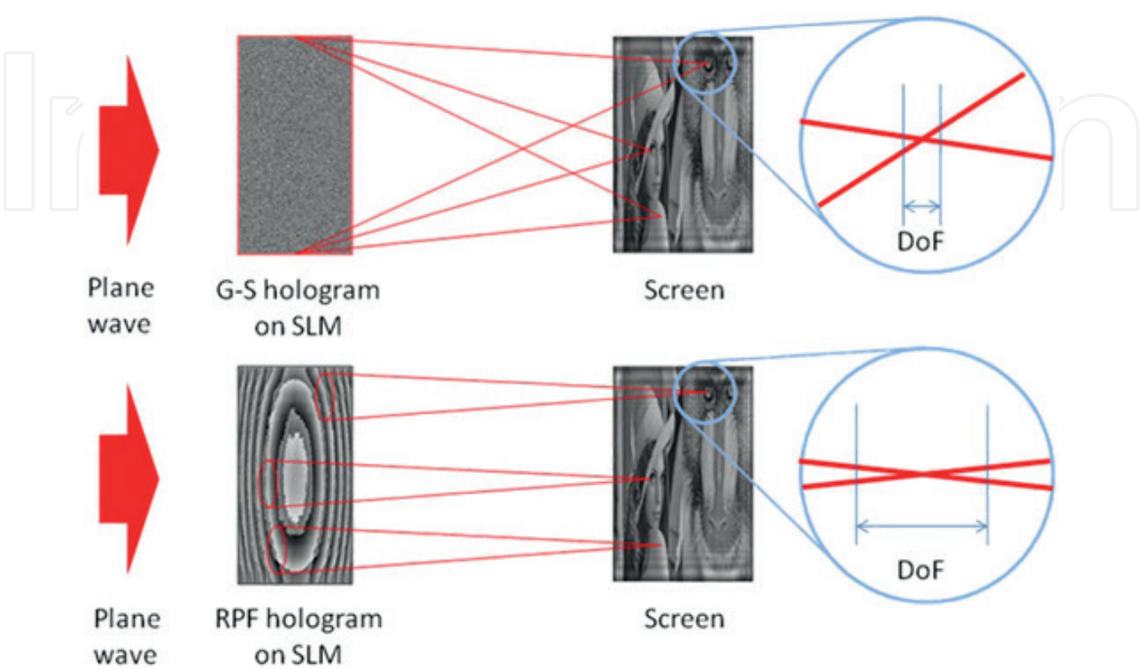

Figure 10.
Comparison of image forming by holograms calculated with G-S and RPF algorithms [10].

by the entire surface of the modulator. In other words, each portion of the SLM creates the entire image—see the upper half of **Figure 10**. In contrast, the ordered phase approach allows the minimal set of frequencies so that each point on the SLM creates only a small portion of the image—in other words, each point of the image is created by a small fraction of the SLM—as shown in the bottom half of **Figure 10**. The big advantage of the ordered phase approach is the smooth and slowly variable phase with sparse zones, as compared to G-S results. Such distributions are easier to be displayed efficiently by the SLM because the number of modulo-2π jumps is much lower and the small differences between the values of adjacent pixels of the SLM minimize the influence of cross-talk, hence increasing the overall diffractive efficiency.

4.2 Depth of focus in holographic projection

The interesting consequence of the varying set of spatial frequencies in CGHs is the different depth of focus of sharp projection. It is much larger in the RPF approach since that configuration can be considered a set of multiple imaging setups of very high F (aperture) numbers. The G-S configuration, on the other hand, can be understood as a single imaging setup with low F-number, and hence the lower depth of focus is natural here. **Figure 11** shows the experimental comparison of both algorithms reconstructing a static image of the *USAF-1951* test pattern at the projection distance of 1000 mm with different intentionally introduced defocus values. Note that the noise amount in RPF is much lower.

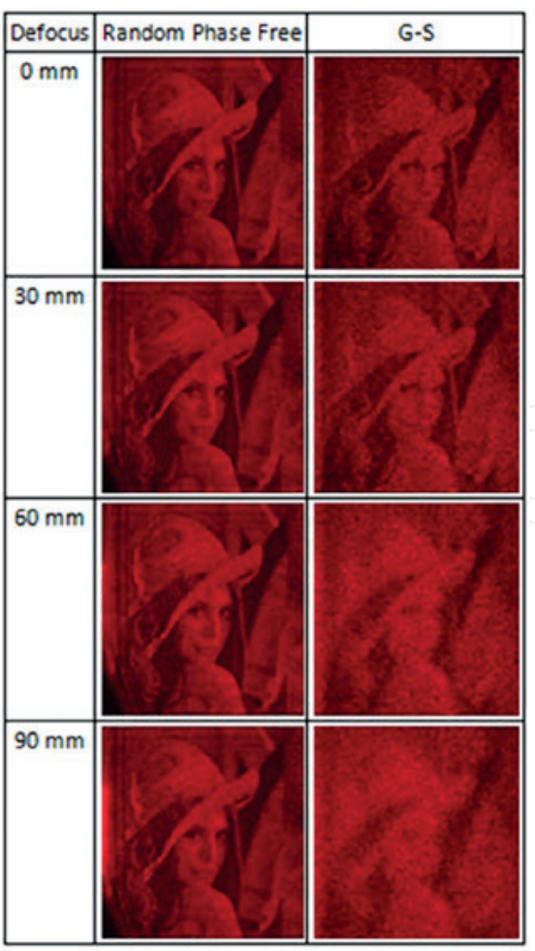

Figure 11.
Comparison of experimental projections from G-S algorithm and RPF algorithm under different defocus for base projection distance of 1000 mm [10].

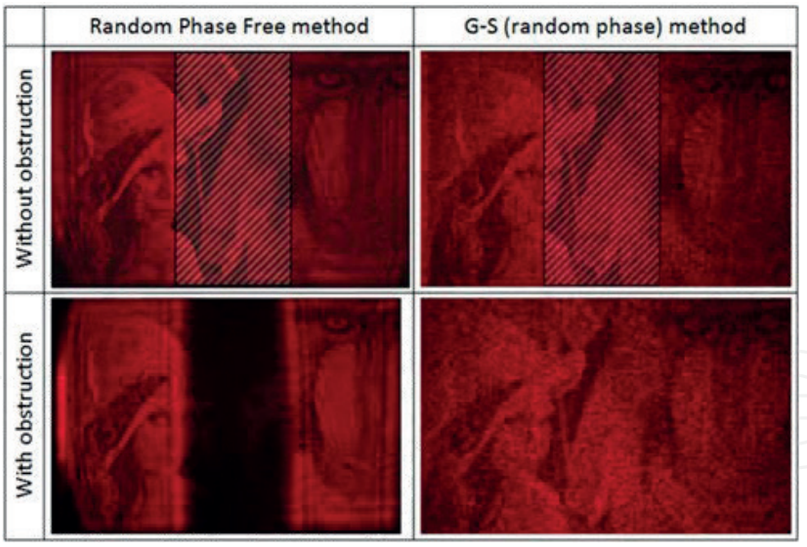

Figure 12.
Resistance to large obstruction of the SLM visible in experimental projections from CGHs calculated with RPF method and G-S method [10].

4.3 Resistance to local defects and obstructions of the SLM

The unique feature of holography is the robustness against any local defects and obstruction at the plane of the light modulator. This is the consequence of the fact that in the diffusive-type CGHs, each point of the image is formed by the whole SLM, therefore obstruction or even a large number of dead pixels is not imaged onto the projected image. This useful feature is especially important for potential applications in portable devices, which tend to wear out and get dirty or damaged. Moreover, from the practical point of view, the quality inspection of SLMs can be far less strict, and fully functional projectors might be constructed from faulty modulators from production rejects. This should lead to greater yield and lower prices of SLMs in the future.

Although the RPF method of CGH computation is superior in many areas, its resistance to local defects on the SLM is much lower than that of the G-S, as shown in **Figure 12**.

This subchapters presents the pros and cons of two different CGH computation algorithms, which belong to a quickly growing class of CGH computation methods [11, 12]. The proper choice of calculation method must meet the requirement and constraints of the planned application [13]. Both algorithms are reasonably simple, based on standard FFT (Fast Fourier Transform) and can be performed in real time on modern GPU (Graphics Processing Unit) processors [9, 14, 46].

5. Improving the quality of holographically projected images

5.1 Image resolution

The number of resolved points in the holographically projected images is close to the number of physical pixels of the SLM taking action in phase modulation, provided that the optical aberrations are carefully taken care of. Thanks to those experimental projections with full HD resolution have been successfully demonstrated [15]. On the other hand, a further increase of the informative capacity of the projected images would require larger arrays of pixels in SLMs with smaller and smaller pixel pitch. Such an approach is very demanding technologically, and the

cross-talk between adjacent SLM pixels [16] would become the dominant effect, compromising the depth and speed of phase modulation. This miniaturization is not to be expected soon enough, therefore another concept of increasing the effective aperture of the SLM was proposed [17].

The Synthetic-Aperture SLM (SASLM) assumes the precise side-by-side positioning of two or more identical SLMs so that under common coherent illumination, they would form a single large SLM from the optical point of view. **Figure 13a** shows the experimental realization of SA-SLM.

The optical flatness of each SLM used in the coherent array is a strict requirement which allows the proper interference of fields coming from SLMs to form a common, high-resolution projected image. This can be measured, for example, with an interferometer and corrected by adding proper corrective phase to the contents on the SLM, as shown in **Figure 13b** and **c**. The use of two SLMs in tandem allows the precise guiding of two beams meeting in the acquisition plane, as seen in **Figure 14**.

The higher localization of a point-spread function spot (PSF) [18] in the Fourier plane of the setup was measured, as shown in **Figure 15**, potentially yielding two-fold increase of image resolution in the direction set by the orientation of the array of SLMs.

5.2 Coherent noise in projected images

Typically, holographically projected images are noisy and there can be named at least two origins of such coherent speckle-like noise. The first one is connected with the speckle noise from a diffuse screen on which the projection takes place. The local roughness of the screen causes uncontrolled interferences when the highly coherent projection beams are diffused toward the viewer's eyes. Numerous

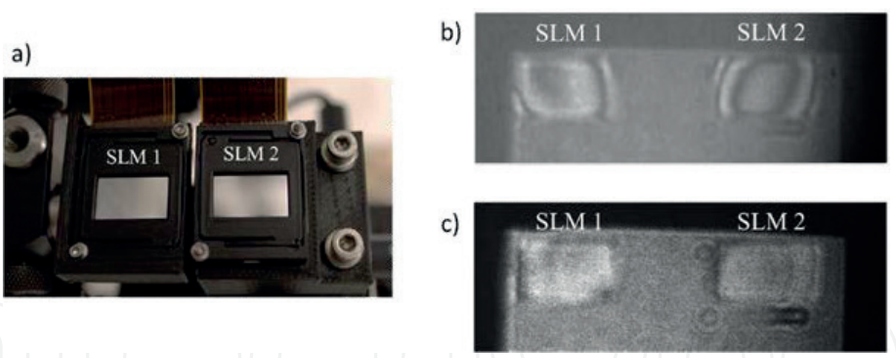

Figure 13.
Experimental setup showing the feasibility of a synthetic-aperture SLM in holographic image projection: (a) precisely positioned SLMs; (b) interferograms of SLMs before correction and (c) after correction [17].

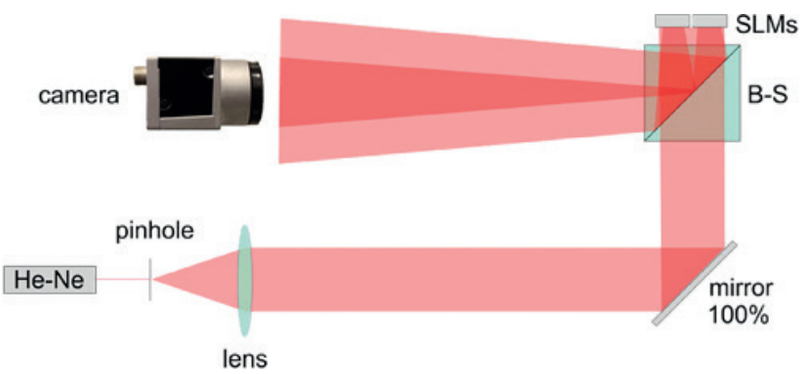

Figure 14.
Optical setup for the realization of improved light focusing by synthetic-aperture SLM [17].

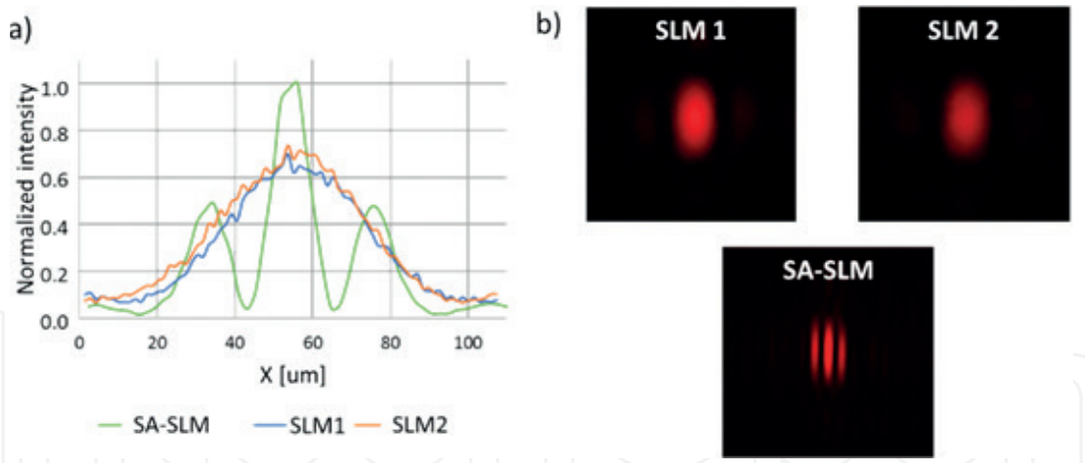

Figure 15.
Experimental measurements of the PSF spot shrunk in the x-direction as a result of synthetic-aperture SLM: (a) cross-sections; (b) captured intensity fields [17].

chapters can be found about the mitigation of such noise, some of them show the use of piezo-actuators to laterally move the screen or a selected optical element inside the projector. Apart from mechanical and polarization-based modulation not much can be done with this source of noise at the stage of design and computation of a CGH.

The other origin of the noise is contained in the algorithm of CGH computation. As a consequence of the phase-only modulation of the SLM, special algorithms of CHG computations must be used which yield unitary amplitude and decent projection quality from the holographic information stored only in the phase component [19, 20]. One of the most popular algorithms is the Gerchberg-Saxton method (see subchapter "Computation of Computer-Generated Holograms"), which uses random phase to create an initial distribution containing a large set of spatial frequencies that the SLM is capable of carrying. In the iterative loop, those frequencies are eliminated based on the constraints in the image plane (usually the image amplitude) and in the SLM plane (usually equal, unitary amplitude). The object information is lost in the process; therefore, the missing frequencies cause speckle noise in the reconstructed images. The physical mechanism behind this phenomenon is the lack of precision in setting the correct phase relations between light rays forming the adjacent image points. Obviously, increasing the number of iterations, one can improve the phase relations and decrease the noise amount, but the computation times then are impractical. Therefore, one must assume the presence of CGH-based noise in holographic projection. The next subchapters will discuss two proposed methods of suppression of this noise, which exploit the long integration time of a human eye and electronic detectors.

5.2.1 Time-domain noise averaging

Initial random phase distribution partly determines the position of phase ambiguity points in the intensity field reconstructed from a CGH. Therefore, the position of bright and dark grains of speckle noise can be altered by re-randomization of the initial phase in the Gerchberg-Saxton algorithm, while the signal information remains unchanged. Therefore, one can quickly display a sequence of holograms of the same object calculated with different initial phase distributions to obtain an effective and simple time-averaging of the noise, which can simulate the partly incoherent illumination [21]. If the speckle noise contrast is defined as:

$$C = \frac{\sigma_I}{<I>}, \tag{3}$$

then the noise averaging technique allows the decrease of C as $\sqrt{N}$, where N is the number of time-integrated frames. In practical experiments, one can decrease the typical noise ratio values from approx. 50% down to 10% by integrating 25 sub-holograms in a single exposure to be examined [22]. **Figure 16** shows exemplary experimental results of such noise integration, combined with piezo-movements of the projection screen.

5.2.2 Pixel separation method

The aforementioned uncontrolled phase relations in the light rays forming adjacent points in the image cause randomly occurring destructive and constructive interferences (see **Figure 17**), which greatly influence the final intensity pattern and thus increase the error [22, 23].

In order to avoid the uncontrolled interferences between closely packed image points, one can separate those points by splitting the input image into its sub-components having regular empty space between pixels, as shown in **Figure 18**. Those subcomponents are then the input images for regular G-S computations and finally are displayed on an SLM in a time sequence, giving a sequence of undisturbed reconstructions.

Obviously, if a fast frame rate SLM is used, the fragmentary images will integrate into the sensor giving the complete image with a very low amount of speckle noise.

The similar technique to time-domain pixel separation is the tiling of the elementary hologram on the surface of the SLM [24, 25] for the price of lowered image resolution.

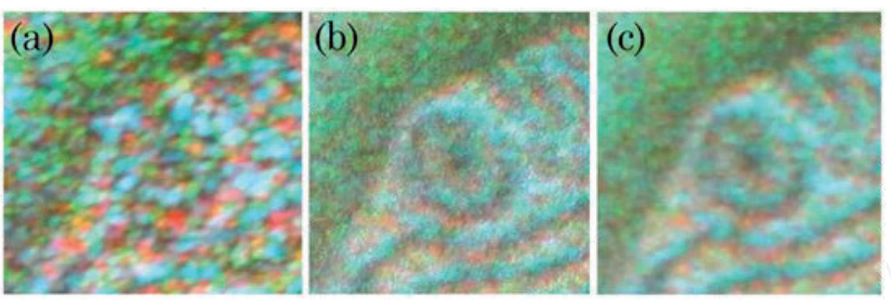

Figure 16.
Close-up of color reconstruction from a CGH computed with the Gerchberg-Saxton algorithm: (a) original image; (b) with time-integration of 25 sub-holograms; (c) with time-integration and piezoelectric movements of the projection screen [7].

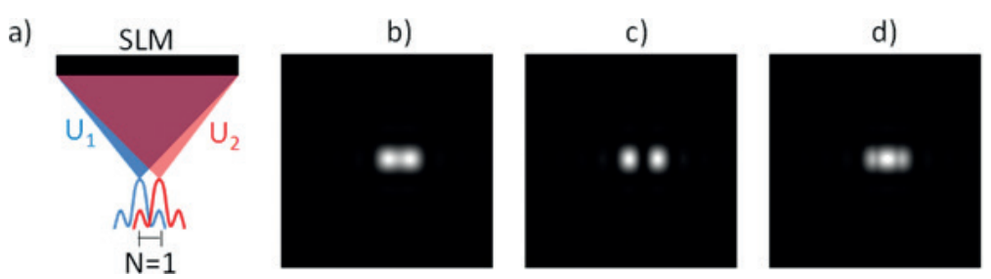

Figure 17.
(a) Interference between fields forming densely packed image points for (b) incoherent illumination; (c) coherent illumination with destructive interference of field between image points; (d) with constructive interference [22].

The comparison of the two presented methods of noise suppression is given in **Figure 19** [22], where the pixel separation methods allow a roughly threefold decrease of noise for the same number of integrations.

Both presented methods require very fast SLMs, therefore are optimal rather for electro-holography based on DLP/DMD [26, 27] or FLCoS (ferroelectric liquid crystal on silicon) modulators [28] with kHz refresh rates. On the other hand, binary phase or amplitude modulation increases the light losses in the holographic process, therefore again a trade-off between efficiency and image quality must be found.

5.2.3 Complex modulation method

The presence of coherent noise is mainly caused by the loss of information by constraining electro-holography to phase-only modulation of light. The attempt to restore complex modulation [6, 29, 30] (i.e., simultaneous amplitude and phase modulation) gives three important advantages in CGH: elimination of speckle noise, faster (i.e., non-iterative) computation and the freedom of phase distribution in the played-back fields. Currently, there are no commercially available complex modulators with appropriate pixel pitch and resolution, therefore one must use at least two separate SLMs and construct an optical setup which would

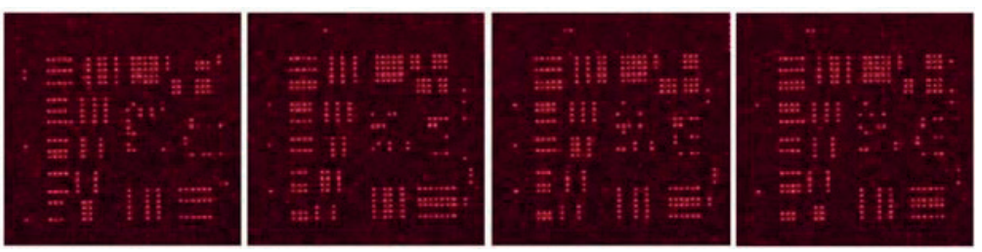

Figure 18.
Reconstructed subcomponents of a USAF-1951 test pattern created for the pixel separation method [22].

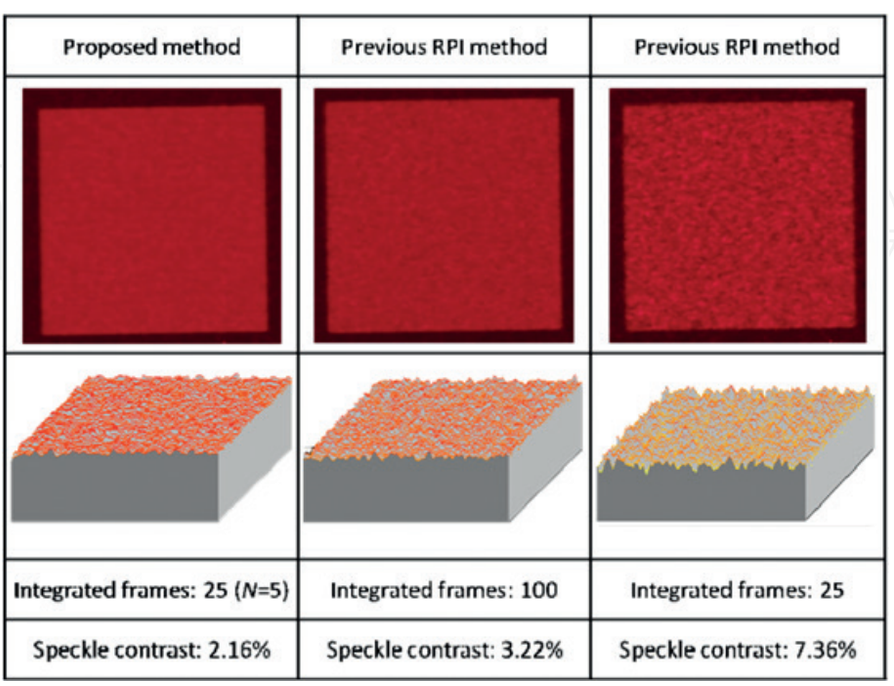

Figure 19.
Comparison of the close-up of the reconstructed uniform area from the USAF-1951 test pattern with the pixel separation method (denoted as "proposed method") and time averaging (RPI—random phase integration) for a different number of integrated sub-holograms [22].

compose them into a single complex modulating plane from the optical point of view. The conceptual scheme of this approach is shown in **Figure 20** [31]. The concept assumes the projection of the desired amplitude of the complex hologram with the use of first SLM on the surface of the other. Then (assuming the pixel-in-pixel positioning) the second SLM adds the proper phase delays of the complex hologram to the process. Then such created complex field propagates toward the projection screen or a detector camera.

It is important to position the SLMs with pixel precision and not to introduce any aberrations to the wave propagating from one SLM to another. For these reasons, the simple imaging of one SLM onto the surface of the other with 1:1 magnification (relay optics) usually introduces too much error and makes the experiment very difficult to adjust [32]. The lack of additional optical elements requires that the CGH computation algorithms take into account the nonzero distance between the SLMs, as seen in **Figure 20**. The numerical propagation at this distance is incorporated into the iterative optimization of the phase of such hologram yielding successful modulation resulting in virtually noiseless reconstructions, see **Figure 21**.

The aberrations caused by the intrinsic curvature of both SLMs must be thoroughly corrected; otherwise, the phase relations would dramatically change in the peripheral areas of the SLMs [32].

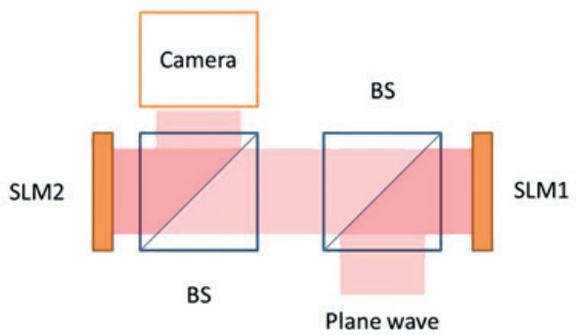

Figure 20.
Conceptual scheme of complex light modulation on two aligned SLMs with two beam-splitter (BS) cubes [31].

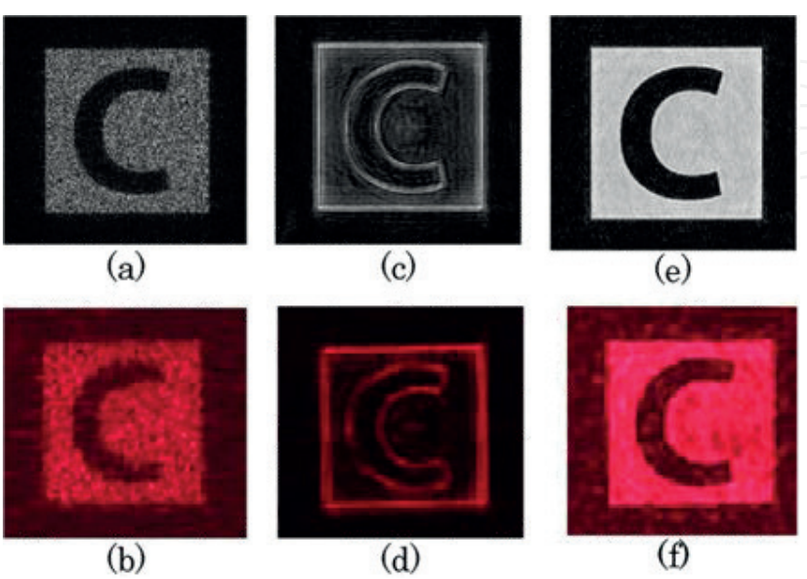

Figure 21.
Exemplary holographic projections from a set of two SLMs performing the complex modulation of light. Numerical simulations of (a) 1-SLM phase-only modulation; (c) 1-SLM phase-only modulation without random initial phase; (e) 2-SLM complex modulation; (b–f) experimental validations [31].

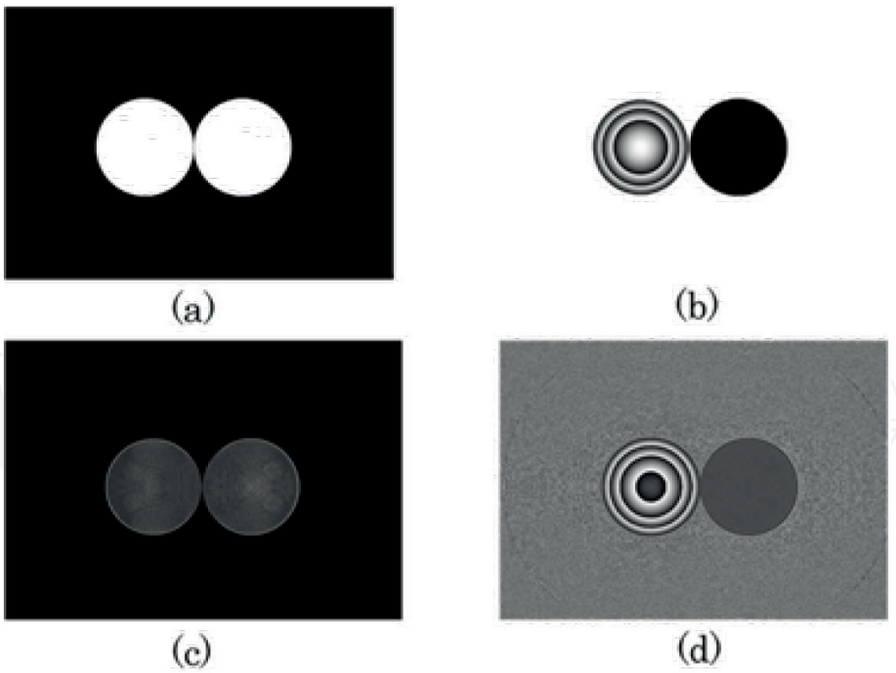

Figure 22.
Numerical simulations of the amplitude and phase projections using computer holography with complex light modulation: (a) desired amplitude; (b) desired phase; (c) numerically projected amplitude; (d) numerically projected phase [32].

The application of complex modulation gives the freedom of adjusting the phase state of the displayed field. Numerical simulations of such holographic reconstructions predict that one could control independently the amplitude and phase at the projection plane, as shown in **Figure 22**. This idea may give significant benefits, for example, in optical trapping and other applications where the spin-momentum of light is of importance.

The described methods of suppression of CGH-based noise should be always combined with the proper choice of the computation algorithm. For example, the RPF algorithm [9] allows virtually noiseless projection.

6. Holographic projection in color

The spatial light modulators are intrinsically monochromatic displays, and all the used rules of diffraction are a constraint to a specific, known wavelength. Without any additional precautions, the strong color mismatch occurs in the holographic projection of color images. As seen in **Figure 2**, the primary components of a projected color image are holographically formed at vastly different angles due to intrinsic chromaticity of the set of diffractive gratings displayed on the SLM. As a first approach, one could use three separate SLMs for the processing of three separate set of holograms, each computed for the given primary wavelength. Nevertheless, this solution greatly complicates the optical setup and implicates higher cost of any projection device. In response to that, this subchapter covers selected methods of displaying color contents with the use of electro-holography on a single SLM. The choice of the optimal method must be based on the characteristics of the SLM. If the frame rate is high the time-division method is favorable, as it allows the full image resolution and extreme simplicity of the illumination. If the SLM lacks fast response and provides a high pixel count, the spatial division method should be considered. The multi-plane method is favorable if high CGH computing power is available on site and the images to be displayed lack high spatial frequencies.

6.1 Compensation of the chromaticity of the SLM

In computer-generated holography, the SLM displays a complex set of diffractive gratings, which obviously diffract different wavelengths at variable angles. The easiest way of quick cancelation of this effect is the initial resize of the color components of the input color image so as to take into account the chromatic dispersion of the process holographic projection. **Figure 23** shows the properly resized and repositioned input images adapted for tilted-illumination projection with the use of three lasers of wavelengths: 633, 532 and 488 nm [33].

6.2 Color holographic projection by time division

The most intuitive and simple way of extending the SLM operation to color imaging is the time division. It assumes the illumination of the whole surface of the SLM in a sequence, for example, Red- > Green- > Blue- > Red- > ... . Obviously, the contents displayed on the SLM must be matched with the illuminating wavelength [34]. This requires quick refresh rates of the SLM because effectively the native frame rate of the panel is divided by three. Practically, the minimal native refresh rate of the SLM is 180 Hz, which allows 60 frames per second of the final color holographic animation. This, in turn, requires the use of especially designed liquid crystal cells [35] or switching to binary ferroelectric LCs [36]. **Figure 24** shows an exemplary experimental holographic projection of color images with the use of time division for pixel separation and color separation.

6.3 Color holographic projection by spatial division

In order to overcome the problem of color breakup and use the full achievable frame rate of the SLM, the spatial division [37, 38] may be used instead of time-division. It involves dividing the SLM into three separated regions illuminated by three beams with associated colors and known wavelengths [39]. **Figure 25** shows the extreme simplicity of this approach [40].

The high-quality color filters are applied directly to the surface of the SLM in order to avoid the cross-talk between regions [41]. Under the filters, three CGHs are displayed side by side, computed with the assumed wavelength, positioned at the projection screen by numerical complex multiplication with proper diffractive gratings and spherical lenses.

The technique is advantageous in a way that computing three smaller holograms is easy to program in parallel graphics processing units (GPU) and field programmable gate array (FPGA) systems [42, 43], and in that, the full frame rate of the SLM is used with no color breakup and smooth color display. This occurs for the inevitable price of lower image resolution due to a limited number of pixels devoted

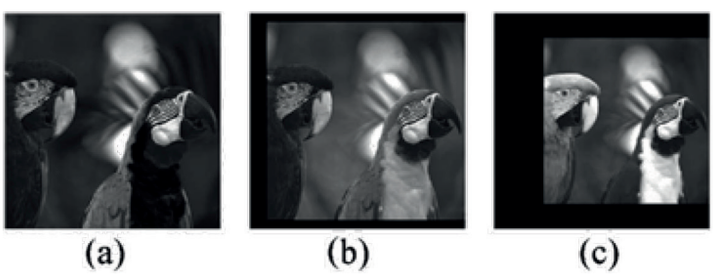

Figure 23.
Resizing and repositioning of the input color components allows quick compensation of the chromaticity of holographic projection: (a) blue component; (b) green component; (c) red component [33].

to the holographic reconstruction of a color component. **Figure 26** shows some exemplary colorful holographic projections [40].

6.4 Multi-plane color hologram

This method combines the advantages of the aforementioned techniques in a way that it utilizes the whole surface and resolution of the SLM in the given moment of time and additionally all three colors are displayed simultaneously [44]. On the other hand, it requires iterative holographic computations and is rather suitable for real-life images with dominant low spatial frequencies.

The chromaticity of SLM is typically a problem, while in this technique, it is treated as a useful phenomenon. First, a CGH containing three amplitude objects located at three distant planes is calculated using the iterative ping-pong algorithm originating from the Gerchberg-Saxton algorithm [45]. When such hologram is

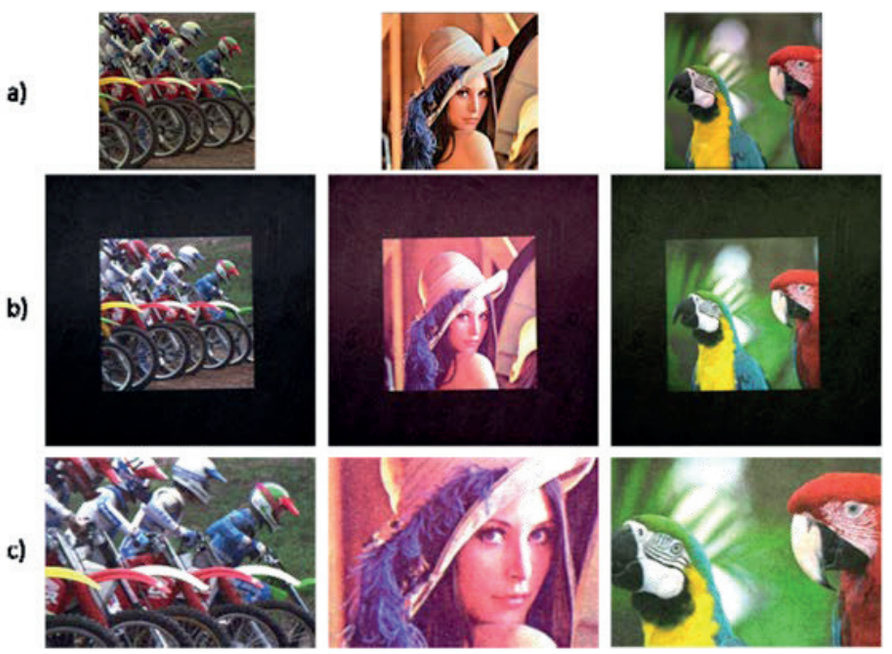

Figure 24.
Exemplary color holographic projections with time division method: (a) input images; (b) captured images; (c) close-ups of the central region showing low noise, high resolution, and good color rendering [22].

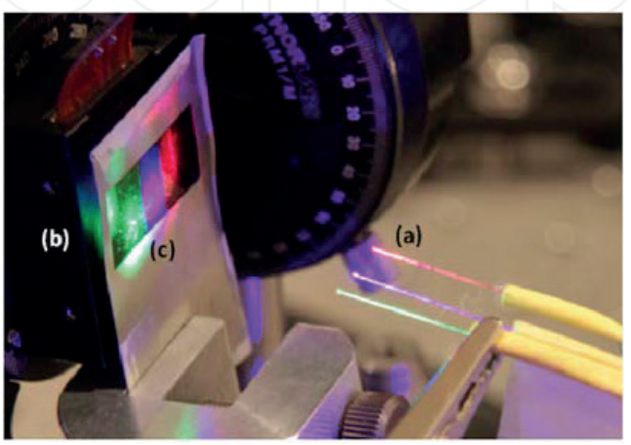

Figure 25.
Spatial division of the SLM: simple illumination with three fibers and color filters: (a) optical fibers; (b) SLM; (c) color filters [40].

reconstructed with a single laser beam of a given wavelength (e.g., red), the three images are played back at projected distances. When a second laser beam of a different wavelength (e.g., green) simultaneously illuminates the SLM, the same images are played back in a different set of distances, according to the chromatic characteristics of the gratings displayed on the SLM. The same happens with the third beam (e.g., blue). One can use the degree of freedom in the choice of propagation

Figure 26.
Exemplary colorful holographic projections achieved with the spatial division method [40].

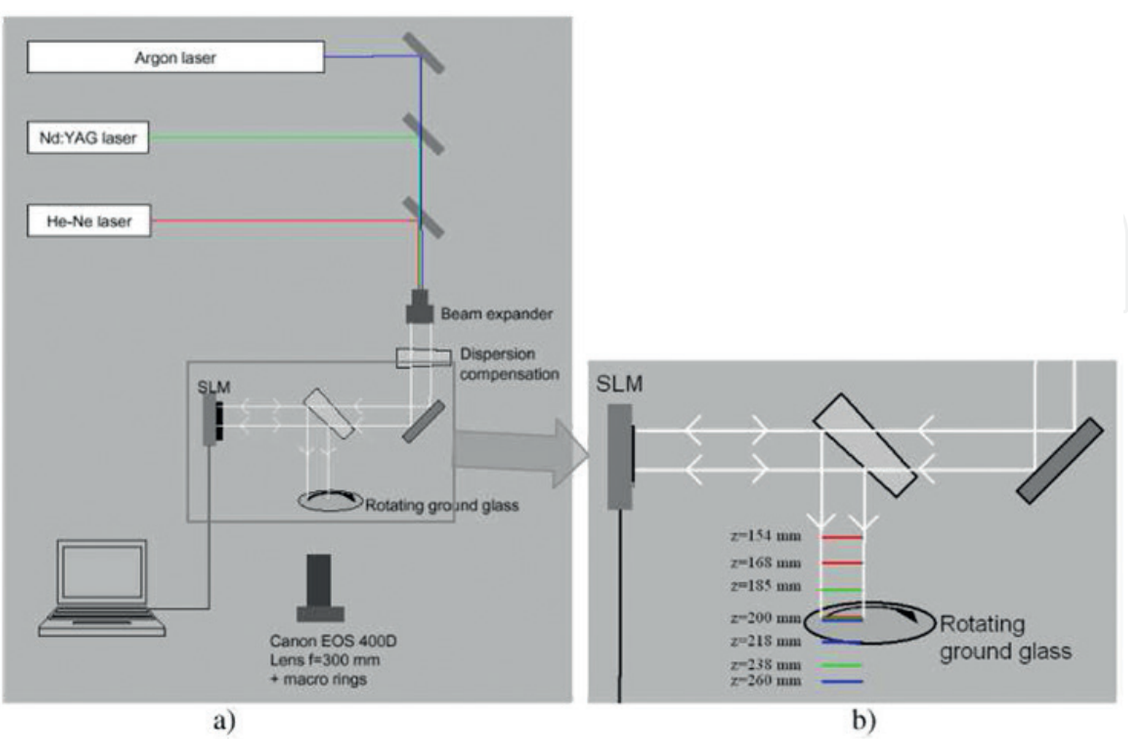

Figure 27.
Reconstruction of the color image at z = 200 mm with simultaneous illumination of the SLM with three wavelengths and displayed multi-plane CGH [44].

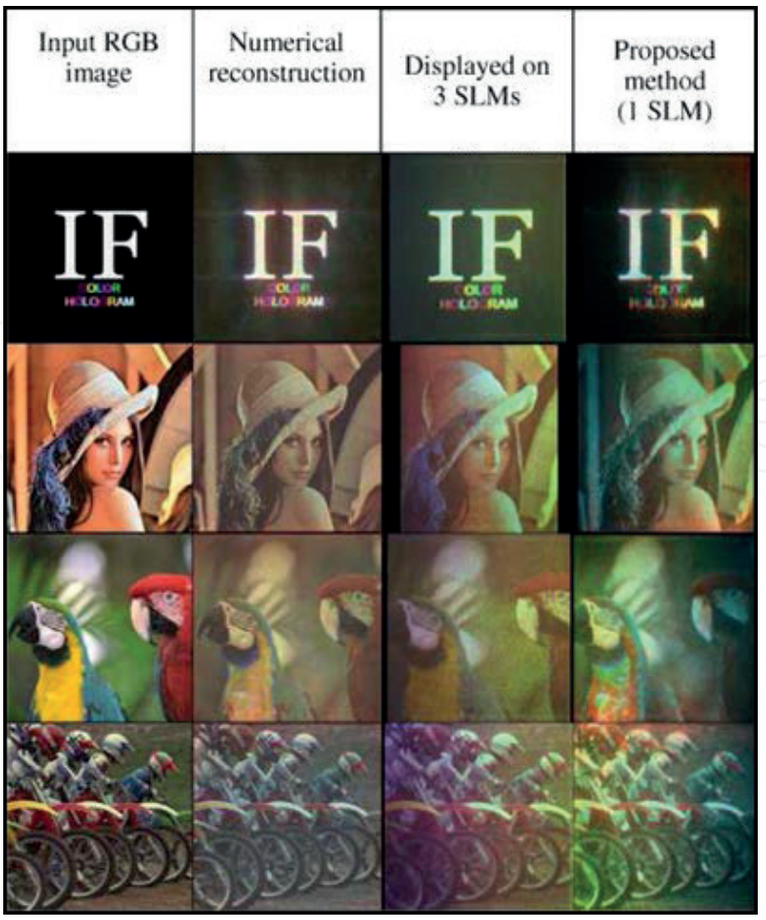

Figure 28.
Exemplary color reconstructions from multi-plane computer-generated hologram [44].

distances of three encoded image planes in order to allow the reconstruction of three images at a fixed plane with three projected wavelengths. This process is depicted in **Figure 27** [44].

The important feature of this method is the simplicity of SLM illumination with three colinear laser beams, which can be easily achieved, for example, with optical fibers [46].

The quality of the color image perceived at the common distance depends on the convergence of the iterative algorithm of CGH computation, which is a constraint for the situation where the color components of the input image are similar. Otherwise, the field creating three very different intensity distributions at such closely packed planes becomes nonphysical and the algorithm fails. The same occurs when the spatial frequencies in any of the three images are too high, which makes the desired light field nonphysical.

Figure 28 shows exemplary color reconstructions from multi-plane holograms. Note the high agreement between the numerical reconstruction and the experimental outcome for most cases. The results are compared with time-sequential color display (denoted as *3 SLMs*) in the figure.

7. Conclusions

Spatial light modulators based on liquid crystals gained popularity in research groups dealing with real-time computer-generated holography. The main reason was the well-established technology of micro-displays known from projectors, monitors, and large screen TVs. On the other hand, their further miniaturization

is problematic because one cannot simultaneously shrink the LC particles, and therefore the smaller and smaller pixel pitch inevitably leads to numerous technical problems like cross-talk, long response, poor fill factor, and flicker. Great effort in many research groups in the world was put to tweak the SLMs and obtain the best possible holographic quality from them, but in the future research of holographic TVs [47] and near-eye displays, their intrinsic hardware drawbacks (like fixed Cartesian pixel array) would be the severe bottleneck.

Next generation of SLMs should be "pixel-less", that is, have freedom of placement and shape [48] of light modulating microareas, and the used medium should not put constraints on the minimal size and dense packing of such "pixels." The problems that remain to be solved is to find the proper medium [49, 50] and the fast and precise method of its addressing, writing, and erasing. Until then, this practical guide to experimental use of LCoS SLMs in computer holography may be used to overcome their current hardware deficiencies.

Acknowledgements

Selected parts of this work were supported by the TEAM-TECH programme of the Foundation for Polish Science co-financed by the European Union under the European Regional Development Fund ("HANEDA", TEAM TECH/2016-3/18, POIR.04.04.00-00-3DD9/16-00).

Conflict of interest

The author declares no conflict of interest.

Author details

Michał Makowski
Warsaw University of Technology, Warsaw, Poland

*Address all correspondence to: michal.makowski@pw.edu.pl

References

[1] Hong K, Oh K, Choo H, Lim Y, Park M. Viewing window position control on holographic projection system by electrically focused tunable lens. Practical Holography XXXII: Displays, Materials, and Applications. 2018;105580R

[2] Wakunami K, Hsieh P, Oi R, Senoh T, Sasaki H, Ichihashi Y, et al. Projection-type see-through holographic three-dimensional display. Nature Communications. 2016;**7**(1):12954

[3] Lizana A, Lobato L, Marquez A, Iemmi C, Moreno I, Campos J, et al. Study of liquid crystal on silicon displays for their application in digital holography. Advanced Holography—Metrology and Imaging. 2011

[4] Cirino GA, Verdonck P, Mansano RD, Pizolato JC Jr, Mazulquim DB, Neto LG. Digital holography: Computer-generated holograms and diffractive optics in scalar diffraction domain. Holography—Different Fields of Application. InTechOpen; 2011

[5] Haist T, Osten W. Holography using pixelated spatial light modulators—Part 1: Theory and basic considerations. Journal of Micro/Nanolithography, MEMS, and MOEMS. 2015;**14**(4):041310

[6] Qi Y, Chang C, Xia J. Speckleless holographic display by complex modulation based on double-phase method. Optics Express. 2016;**24**(26):30368

[7] Makowski M, Ducin I, Kakarenko K, Kolodziejczyk A, Siemion A, Siemion A, et al. Efficient image projection by Fourier electroholography. Optics Letters. 2011;**36**(16):3018

[8] Makowski M, Kowalczyk A, Bieda M, Suszek J, Ducin I, Shimobaba T, et al. Miniature holographic projector with cloud computing capability. Applied Optics. 2019;**58**(5):A156

[9] Shimobaba T, Ito T. Random phase-free computer-generated hologram. Optics Express. 2015;**23**(7):9549

[10] Makowski M, Shimobaba T, Ito T. Increased depth of focus in random-phase-free holographic projection. Chinese Optics Letters. 2016;**14**(12):120901-120905

[11] Mengu D, Ulusoy E, Urey H. Non-iterative phase hologram computation for low speckle holographic image projection. Optics Express. 2016;**24**(5):4462

[12] Duan J, Liu J, Hao B, Zhao T, Gao Q, Duan X. Formulas of partially spatial coherent light and design algorithm for computer-generated holograms. Optics Express. 2018;**26**(17):22284

[13] Chang C, Wu J, Qi Y, Yuan C, Nie S, Xia J. Simple calculation of a computer-generated hologram for lensless holographic 3D projection using a nonuniform sampled wavefront recording plane. Applied Optics. 2016;**55**(28):7988

[14] Shiraki A, Takada N, Niwa M, Ichihashi Y, Shimobaba T, Masuda N, et al. Simplified electroholographic color reconstruction system using graphics processing unit and liquid crystal display projector. Optics Express. 2009;**17**(18):16038

[15] Makowski M, Ducin I, Kakarenko K, Suszek J, Kowalczyk A. Performance of the 4k phase-only spatial light modulator in image projection by computer-generated holography. Photonics Letters of Poland. 2016;**8**(1):26-28

[16] Persson M, Engström D, Goksör M. Reducing the effect of pixel crosstalk

in phase only spatial light modulators. Optics Express. 2012;**20**(20):22334

[17] Kowalczyk A, Makowski M, Ducin I, Sypek M, Kolodziejczyk A. Collective matrix of spatial light modulators for increased resolution in holographic image projection. Optics Express. 2018;**26**(13):17158

[18] Běhal J, Bouchal Z. Optimizing three-dimensional point spread function in lensless holographic microscopy. Optics Express. 2017;**25**(23):29026

[19] Chang C, Qi Y, Wu J, Xia J, Nie S. Speckle reduced lensless holographic projection from phase-only computer-generated hologram. Optics Express. 2017;**25**(6):6568

[20] Utsugi T, Yamaguchi M. Speckle-suppression in hologram calculation using ray-sampling plane. Optics Express. 2014;**22**(14):17193

[21] Czerwiński A, Kakarenko K, Sypek M, Makowski M, Ducin I, Suszek J, et al. Modeling of the optical system illuminated by quasi-monochromatic spatially incoherent light: New numerical approach. Optics Letters. 2012;**37**(22):4723

[22] Makowski M. Minimized speckle noise in lens-less holographic projection by pixel separation. Optics Express. 2013;**21**(24):29205

[23] Mori Y, Fukuoka T, Nomura T. Speckle reduction in holographic projection by random pixel separation with time multiplexing. Applied Optics. 2014;**53**(35):8182

[24] Georgiou A, Christmas J, Moore J, Jeziorska-Chapman A, Davey A, Collings N, et al. Liquid crystal over silicon device characteristics for holographic projection of high-definition television images. Applied Optics. 2008;**47**(26):4793

[25] Makowski M, Kakarenko K, Ducin I, Kowalczyk A, Bieda M, Suszek J. Study of image resolution in holographic projection. Photonics Letters of Poland. 2014;**6**(3):96-98

[26] Su P, He Z, Ma J, Cao L, Yuan R. Design of color LED holographic display system based on DMD. Digital Holography and Three-Dimensional Imaging. 2016:W2A-16

[27] Park M, Lee B, Son J, Chernyshov O. Properties of DMDs for holographic displays. Journal of Modern Optics. 2015;**62**(19):1600-1607

[28] Schmieder F, Klapper S, Koukourakis N, Busskamp V, Czarske J. Optogenetic stimulation of human neural networks using fast ferroelectric spatial light modulator—Based holographic illumination. Applied Sciences. 2018;**8**(7):1180

[29] Cao L, Kong D, Zong S, Zhang H, Jin G, Xueju S. Complex wavefront modulation and holographic display using single spatial light modulator. Optics and Photonics for Information Processing XI. 2017:1039508

[30] Luis Martínez Fuentes J, Moreno I. Random technique to encode complex valued holograms with on axis reconstruction onto phase-only displays. Optics Express. 2018;**26**(5):5875

[31] Siemion A, Sypek M, Suszek J, Makowski M, Siemion A, Kolodziejczyk A, et al. Diffuserless holographic projection working on twin spatial light modulators. Optics Letters. 2012;**37**(24):5064

[32] Makowski M, Siemion A, Ducin I, Kakarenko K, Sypek M, Siemion AM, et al. Complex light modulation for lensless image projection. Chinese Optics Letters. 2011;**9**(12):120008-120010

[33] Makowski M, Ducin I, Sypek M, Siemion A, Siemion A, Suszek J,

et al. Color image projection based on Fourier holograms. Optics Letters. 2010;**35**(8):1227

[34] Han Z, Yan B, Qi Y, Wang Y, Wang Y. Color holographic display using single chip LCOS. Applied Optics. 2018;**58**(1):69

[35] Holoeye LETO SLM. Available from: https://holoeye.com/spatial-light-modulators/leto-phase-only-spatial-light-modulator/ [Accessed: January 20, 2019]

[36] ForthDD Products. Available from: https://www.forthdd.com/products/spatial-light-modulators/ [Accessed: January 20, 201901-20]

[37] Zaperty W, Kozacki T, Gierwiało R, Kujawińska M. RGB imaging volumes alignment method for color holographic displays. Photonics Applications in Astronomy, Communications, Industry, and High-Energy Physics Experiments. 2016:1003117

[38] Zaperty W, Kozacki T, Kujawinska M. Multi-SLM color holographic 3D display based on RGB spatial filter. Journal of Display Technology. 2016;**12**(12):1724-1731

[39] Shimobaba T, Takahashi T, Masuda N, Ito T. Numerical study of color holographic projection using space-division method. Optics Express. 2011;**19**(11):10287

[40] Makowski M, Ducin I, Kakarenko K, Suszek J, Sypek M, Kolodziejczyk A. Simple holographic projection in color. Optics Express. 2012;**20**(22):25130

[41] Tsuchiyama Y, Matsushima K. Full-color large-scaled computer-generated holograms using RGB color filters. Optics Express. 2017;**25**(3):2016

[42] Yamamoto Y, Nakayama H, Takada N, Nishitsuji T, Sugie T, Kakue T, et al. Large-scale electroholography by HORN-8 from a point-cloud model with 400,000 points. Optics Express. 2018;**26**(26):34259

[43] Shimobaba T, Ito T. Computer Holography: Acceleration Algorithms and Hardware Implementations. 1st ed. Boca Ranton, USA: CRC Press; 2019

[44] Makowski M, Sypek M, Ducin I, Fajst A, Siemion A, Suszek J, et al. Experimental evaluation of a full-color compact lensless holographic display. Optics Express. 2009;**17**(23):20840

[45] Gerchberg RW, Saxton WO. A practical algorithm for the determination of phase from image and diffraction plane pictures. Optik (Jena). 1972;**35**:237-246

[46] Kowalczyk A, Bieda M, Makowski M, Sypek M, Kolodziejczyk A. Fiber-based real-time color digital in-line holography. Applied Optics. 2013;**52**(19):4743

[47] Reichelt S, Haussler R, Leister N, Futterer G, Stolle H, Schwerdtner A. Holographic 3-D displays—Electro-holography within the grasp of commercialization. Advances in Lasers and Electro Optics. InTech; 2010

[48] Xiao Ma X, Juan Liu J, Zhao Zhang Z, Xin Li X, Jia Jia J, Bin Hu B, et al. Analysis of optical characteristics of modulation devices with square and circle pixels for 3D holographic display. Chinese Optics Letters. 2015;**13**(1):010901-010905

[49] Kveton M, Fiala P, Havranek A. Polymer holography in acrylamide-based recording material. Holography, Research and Technologies. IntechOpen; 2011

[50] Stupakiewicz A, Szerenos K, Afanasiev D, Kirilyuk A, Kimel A. Ultrafast nonthermal photo-magnetic recording in a transparent medium. Nature. 2017;**542**(7639):71-74